Characteristics and mechanism of time on sand powder 3D printing rock analogue: a new method for fractured rock mechanics

**Zhe Zhang · Lishuai Jiang · Chunang Li ·
Yang Zhao · Atsushi Sainoki · Xuanlin Gong**

Abstract Laboratory tests are one of the most fundamental and crucial methods in rock mechanics and engineering research. Natural rock specimens are challenging to acquire, and traditional casting methods involve prolonged curing times and cannot produce rock-like specimens with complex internal fractures. Furthermore, 3D printing technologies such as SLA, SLS, and FDM possess inherent limitations. In this study, high-silica sand was used as the printing material, and sand powder 3D printing technology was harnessed to fabricate rock-like specimens. Uniaxial compression tests were performed on specimens with varying placement times, aimed at investigating the impact of placement time on the mechanical properties of sand 3D-printed rock-like specimens. Acoustic emission technology was used to explore the internal state changes during deformation and failure of specimens with different placement times. The findings indicate that the mechanical properties of sand powder 3DP rock-like specimens exhibited no deterioration over time after approximately 7 days of placement. The internal structure remained unchanged across different placement times. This study's outcomes underscore the superiority of sand powder 3D printing technology within the realm of rock mechanics and establish the groundwork for the accurate and efficient fabrication of rock-like specimens through sand powder 3D printing technology in the future.

Keywords Sand powder 3D printing · Rock-like material · Rock mechanics · Fractured rock mass

Z. Zhang · L. Jiang (✉) · C. Li · Y. Zhao (✉)
College of Energy and Mining Engineering, Shandong
University of Science and Technology, Qingdao 266590,
China
e-mail: lsjiang@sdust.edu.cn

Y. Zhao
e-mail: mrzhao_y@163.com

Z. Zhang · L. Jiang · C. Li · Y. Zhao
State Key Laboratory of Mining Disaster Prevention
and Control, Shandong University of Science
and Technology, Qingdao 266590, China

A. Sainoki
Faculty of Advanced Science and Technology, Kumamoto
University, Kumamoto 860-8555, Japan

A. Sainoki
International Research Organization for Advanced
Science and Technology, Kumamoto University,
Kumamoto Kumamoto, Japan

X. Gong
Department of Mining and Materials Engineering, McGill
University, Montreal H3A 0E8, Canada

1 Introduction

In the field of geomechanics for geo-resources, one of the greatest challenges are the existence of joints or other kinds of discontinuities (faults, fractures, cracks, bedding planes, etc.) in encountered rock or strata. It is well believed that the mechanical

behaviors of jointed rock mass have significant effect on the stability of rock excavation and thereby influence the safe and efficient extraction of deep geo-resources. (Cao et al. 2016; Cacciari and Futai 2022; Zhao et al. 2023).

Presently, the predominant methods for exploring these properties within complex rock masses involve on-site monitoring (Herget and Unrug 1976; Gehlin 1998; Nizametdinov et al. 2016; Wang et al. 2021a, b), numerical simulation (Goodman et al. 1968; Barton 1972; Barton et al. 1985; Hart 2003; Kim et al. 2018; Ma et al. 2023), and laboratory testing (Kovari et al. 1983; Nicksiar and Martin 2012; Feng et al. 2019; Mangs et al. 2022; Tang et al. 2022). Among these approaches, laboratory tests are continually held in high regard, representing one of the most fundamental and pivotal avenues for comprehending rock mechanics and engineering (Jiang et al. 2022). Nevertheless, the study of natural coal-rock masses presents unique challenges due to their intricate mineral compositions and extensively developed joint fractures, which complicate the task of preparing genuine rock specimens. Moreover, given the material heterogeneity of specimens, the inherent randomness of internal structures, and the inherently invasive nature of laboratory tests, coupled with the application of actual rock fracturing techniques like high-pressure water cutting (Li et al. 2019) and diamond sawing (Yan et al. 2021), the specimens can experience structural disturbances and impairment. Consequently, even samples extracted from one rock body can exhibit pronounced dispersion and inherent uncertainties in the test outcomes.

To tackle the challenge of limited experimental materials, researchers have resorted to using analogous materials for crafting rock-like specimens, aiming to replicate the characteristics of genuine rock specimens. (Cao et al. 2019) For example, Cao et al. (2015) investigated the phenomenon of fracture coalescence, which plays a crucial role in the behavior of brittle materials, by loading rock-like specimens with two and three pre-existing flaws created by extracting embedded metal inserts during the pre-curing period. Sun et al. (2019) conducted a study by examining rock-like specimens with conjugate fractures, altering the horizontal angle and length, and analyzing the physical parameters and fracture modes under uniaxial compression testing. They also compared these results with those obtained from simulation

analysis. From these studies, it becomes apparent that while the pouring method aids in mitigating the influence of rock heterogeneity on test outcomes (Dyskin et al. 2003; Haeri et al. 2015; Fedrizzi et al. 2018), it remains constrained by its inability to emulate intricate geometrically-shaped fractures within specimens. Instead, it can only replicate basic fractures through the inclusion of steel plates or wire cutting. Consequently, the crux of surmounting the limitations of traditional rock mechanics testing lies in the precise, efficient, and reproducible preparation of specimens that authentically mirror the genuine mechanical and structural properties inherent in coal-rock.

In recent years, the rapid advancement of 3D printing technology has emerged as a potential solution for mass-producing intricately structured three-dimensional models, offering a promising solution to the scarcity of suitable objects for rock mechanics testing (Zheng et al. 2019; Almetwally and Jabbari 2020; Gao et al. 2021; Wang et al. 2022a, b; Liu et al. 2022). Leveraging 3D printing technology enables the swift and precise creation of rock-like specimens that closely resemble real rock structures. When coupled with CT scanning and computer-aided modeling, it even opens the door to producing rock-like specimens that faithfully replicate the internal flaws found in original samples (Gao et al. 2021; Jiang et al. 2022). As 3D printing technology continues to evolve, an increasing number of scholars have recognized its pivotal role in rock mechanics research, resulting in numerous pioneering investigations. Ju et al. (2014; 2017a, b), for instance, employed CT imaging, 3D reconstruction, and stereolithography (SLA) to craft natural coal-rock specimens characterized by intricate fractures. This approach visually showcased stress field distribution within fractured coal-rock under load, offering transparent insights into the discontinuous structure and physical field effects underlying rock disasters. In the case of Zhu et al. (2018, 2020), a comparative analysis of various 3D printing technologies was conducted through uniaxial compression tests, highlighting that specimens produced via SLA technology are adept at simulating hard rocks. Similarly, Vălean et al. (2020), JIANG (Jiang and Zhao 2015; Jiang et al. 2016a, b), and others harnessed FDM technology and polylactic acid (PLA) to create rock-like specimens exhibiting diverse crack features. Test outcomes revealed

limitations in mechanical properties of specimens made with FDM technology and PLA material, hindering their direct simulation of natural rocks. Wang et al. (2021a, b), on the other hand, employed gypsum powder as the primary material to generate 3D printed rock-like specimens featuring isolated cracks and intact joints. Experimental results demonstrated this material's unique dual traits, manifesting as low strength and pronounced plastic deformation due to its high porosity. In sum, while photopolymerization technology proves suitable for emulating robust natural rocks, disparities between specimens and rock compositions present challenges in modifying their rock-like attributes. FDM technology and PLA material face limitations when simulating natural rocks, while gypsum powder printed specimens are confined by their mechanical properties and struggle to accurately replicate natural rock qualities. Therefore, the quest for appropriate printing technology and materials remains imperative to address the aforementioned issues.

In comparison to specimens generated through alternative printing technologies, sand powder 3D printed rock-like specimens possess distinct advantages, including a close resemblance to the original rock composition, evident pore structures, and realistic surface roughness. Researchers such as Gomez et al. (2019), Vogler et al. (2017), Jiang et al. (2016a, b), Zhang and Li (2022), Zhang et al. (2023) and Wang et al. (2022a; b) employed sand powder 3D printing technology to craft specimens and subsequently conducted uniaxial compression and Brazilian disc tests. These investigations revealed that such sand powder 3D printed rock-like specimens exhibit similar crucial mechanical parameters and failure modes as natural rocks, though their peak strength and elastic modulus tend to be lower. Building upon these findings, Jiang et al. (2022), Xu et al. (2021) and Niu et al. (2023) delved into the impact of sand powder type, printing layer thickness, printing direction, binder concentration, and post-processing temperature on sand powder 3D printed rock-like specimens. Through alterations to sand powder type and binder parameters in sand 3D printing technology, the peak strength of the specimens was nearly doubled compared to conventional sand powder 3D printed rock-like specimens. This successful modification enabled the production of specimens mirroring the characteristics of

softer rocks, such as coal and mudstone. Additionally, Tian et al. (2023) made significant strides in surmounting the inherent limitations of low strength and stiffness in sand powder 3D printed rock-like specimens. This was achieved by employing four distinct post-processing methods: high-temperature baking, vacuum infiltration, low-temperature treatment, and vacuum infiltration at low temperature. Consequently, a broader spectrum of natural rock properties could be accurately replicated.

Presently, the viability and advantages of sand powder 3D printing technology in rock mechanics research have been substantiated by an array of scholars, following their extensive investigations. Nevertheless, considering material characteristics and mechanical attributes, noteworthy distinctions between 3D printed rock-like specimens and their natural rock counterparts still persist. Consequently, additional research on sand powder 3D printed rock-like specimens remains imperative to elucidate the intricate interplay between diverse influencing factors and the resultant peak strength of these specimens.

Therefore, building upon prior research, the primary objective of this study is delving into the impact of various placement time on the mechanical attributes of sand powder 3D printed rock-like specimens. We will accomplish this by conducting a series of experiments, including uniaxial compression tests, acoustic emission (AE) analysis, and observation through scanning electron microscopy. Our research aims to uncover how different placement times impact both the internal structure and mechanical characteristics of these specimens. The research outcomes hold noteworthy implications, offering valuable insights into the refined and more efficient fabrication of rock-like specimens that closely mirror the mechanical characteristics of authentic rocks.

2 Specimen preparation and experimental design

2.1 Specimen preparation

The 3D printing equipment employed in this test is the Easy3DP-S450 printer, as shown in Fig. 1, manufactured by Wuhan Easy3DP Technology Co., Ltd. The dimensions of the molding cylinder are $500 \times 450 \times 400$ mm, while the minimum printing layer thickness is 0.05 mm, and the printing speed

Fig. 1 Easy3DP-S450 printer

ranges from 7 to 25 s/layer. This equipment is outfitted with a piezoelectric imported sprinkler head, boasting a maximum physical resolution of 720 DPI.

Based on a comprehensive review of existing literature and prior comparative research and testing involving sand 3D printed rock-like materials, it has been ascertained that rock-like specimens crafted from high-silica sand exhibit a high degree of similarity to coal-rock specimens in terms of strength characteristics and fracture patterns (Bertuzzi and Pells2002; Vogler et al. 2017; Kong et al. 2018a, b; Perras and Vogler 2019; Song et al. 2020; Xu et al. 2021; Barbosa et al. 2022; Jiang et al. et al. 2022; Niu et al. 2023). As a result, the choice of printing material fell upon high-silica sand, featuring particle sizes ranging from 0.075 to 0.15 mm. In the printing process, furan resin was employed as the binding agent, primarily incorporating an acid curing agent of toluene sulfonic acid. Detailed printing parameters are provided in Table 1.

The printing process can be divided into several steps: (1) Import the pre-designed digital model into

Table 1 Print parameter

Binder	Curing agent	Thickness	The proportion of sand and curing agent	The binder concentration	Sand size
Furan resin	Toluene sulfonic acid	0.25 mm	1000:3	50%	0.075–0.15 mm

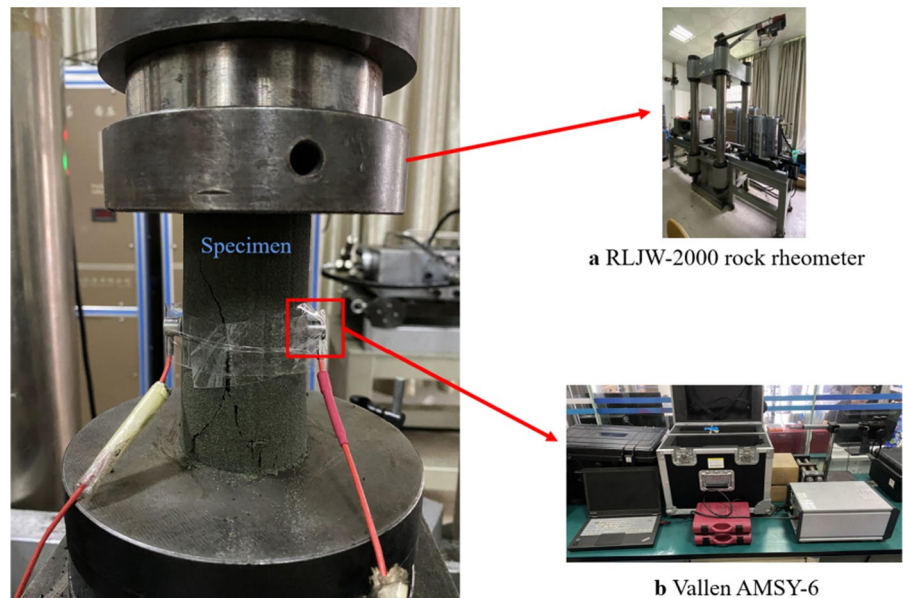**Fig. 2** The functional diagram of 3D printing processes (Zhao et al 2023)
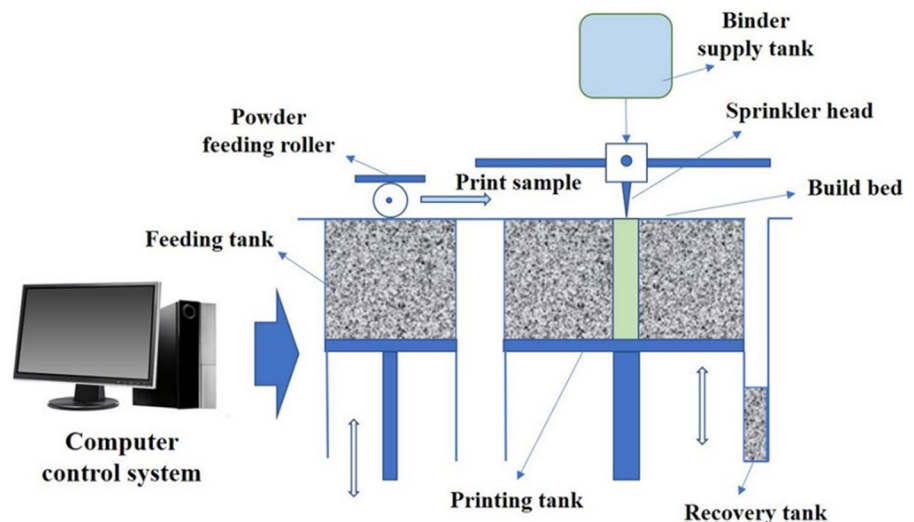
the printer; (2) Introduce the powder mixture containing the curing agent into the feeding tank; (3) Evenly distribute the powder across the base of the printing tank to prevent contact between the forming specimen and the tank's bottom; (4) Initiate the printing procedure; (5) Retrieve the fully formed specimen once printing is complete. The functional diagram of 3D printing processes is shown in Fig. 2.

During the process of getting the printed specimen, it was found that the upper part of the newly printed cylindrical specimen was relatively soft and had a certain temperature. This is because the reaction between furan resin and curing agent is an exothermic reaction. During the initial stage of forming and curing, the furan resin and curing agent between the sand particles in the upper part of the specimen have not fully reacted, and the bonding material between the particles has not solidified. The heat generated by the reaction has not dissipated. After about 0.5 h of forming and curing, the overall temperature of the specimen becomes uniform and equal to room temperature, and the specimen solidifies basically.

2.2 Test design and equipment

Sample preparation was carried out 44 days, 30 days, 17 days, 7 days, and 1 day before the start of the test. This allowed for obtaining specimens that had been placed for 1 day, 7 days, 17 days, 30 days, and 44 days

prior to the commencement of the test. The trio of specimens left for 1 day were labeled D1-1, D1-2, and D1-3 in sequence, with corresponding nomenclature for the remaining specimens. Subsequently, the specimens underwent uniaxial compressive tests alongside acoustic emission assessments, as shown in Fig. 3. Due to the low strength of the sand 3D printed specimens, the displacement control method was used in this test, with a loading rate of 0.3 mm/min. The axial strain was recorded using an external displacement sensor attached to the testing machine. This combined approach aimed to probe the influence of varying placement times on the uniaxial compressive strength and the internal damage evolution characteristics of the specimens. Upon the conclusion of the uniaxial compression tests, rock slices were extracted from the fracture surfaces of each specimen group. The granular structures at these fracture surfaces were then subjected to scanning utilizing a field emission scanning electron microscope.

3 Experimental results and analysis

3.1 Analysis of surface appearance and mass changes of the specimens

After different periods of placement, noticeable changes were observed on the surface of the sand 3D


Fig. 3 Experimental process and equipment

a RLJW-2000 rock rheometer

b Vallen AMSY-6

Fig. 4 Sand powder 3D printed rock-like specimen after different placement times
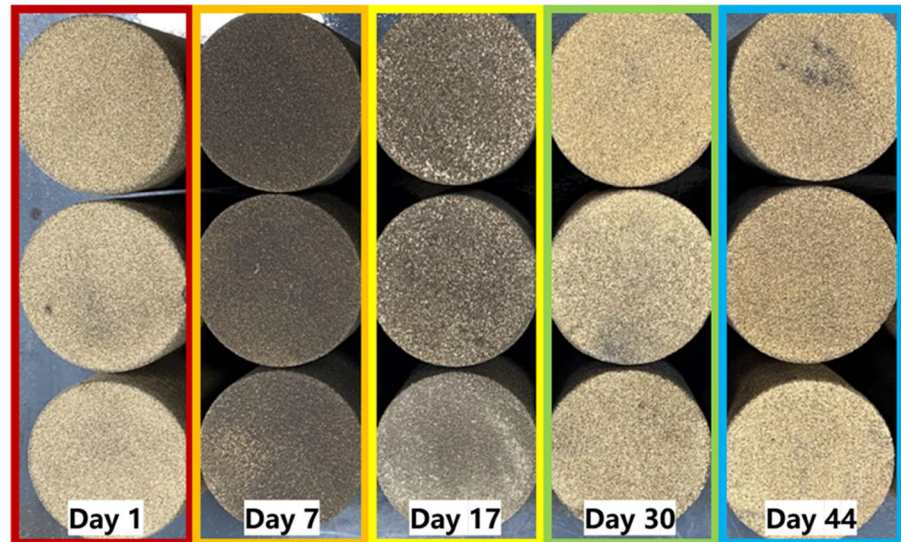
printed rock-like specimens. As shown in Fig. 4, after the specimens were printed and placed for 1 day, the surface appeared bluish-green. Scratching the surface with a hard object caused scratches and a small amount of sand particles to come off. This was due to the incomplete curing of the furan resin between the sand particles. After 7 days, the specimens appeared dark gray-black, and scratching the surface did not result in any sand particle detachment. This was because the furan resin inside the specimens had reacted with the acidic curing agent in 7 days. After 17 days, partial oxidation occurred on the surface of

the specimens, forming a thin oxide layer. The surface appearance of the specimens changed from black-brown to light black–brown through the yellow–brown oxide layer. However, the dark gray–black color was still visible beneath the oxide layer. Scratching the surface with a hard object did not cause any sand particle detachment. After 30 days, the oxide layer on the surface of the specimens expanded and slightly thickened. The yellow–brown oxide layer gradually spread to the entire surface of the specimens, with only a small area remaining uncovered by the oxide layer. After 44 days, the surface appearance

Fig. 5 Comparison of oxidized side and unoxidized side of specimen
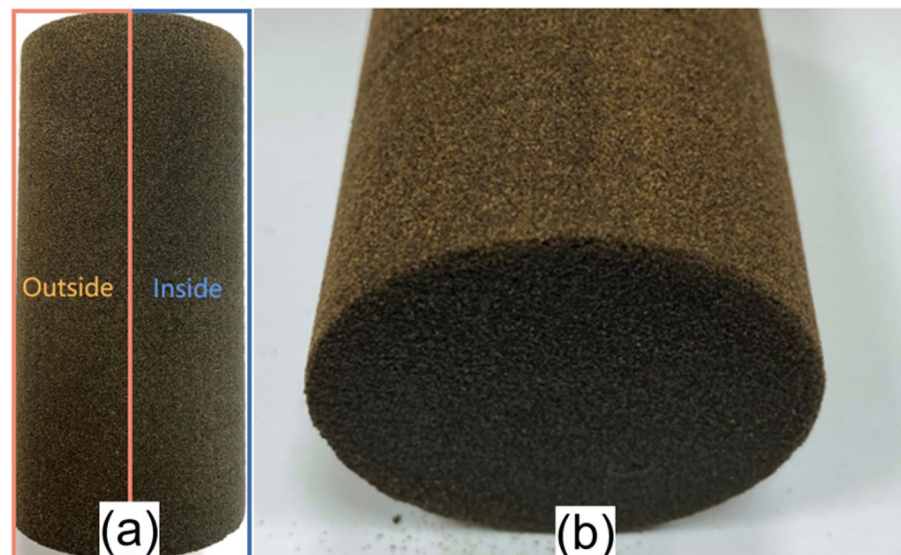
of the specimens changed from yellow–brown to light reddish-brown. The oxide layer on the surface thickened, but only a very small amount of sand particles detached when the oxide layer was rubbed with a hard object.

Over time, during the period of concentrated placement, only the surface areas of the specimens that were in direct contact with the external environment exhibited signs of oxidation, with no significant oxide layer forming internally or at the bottom of the specimens. As shown in Fig. 5, when subjected to a concentrated placement of 44 days without any additional treatment at room temperature, a distinct demarcation line was visible between the inner and outer regions of the specimens. The outer sides and top surfaces of the specimens displayed a noticeable light reddish-brown oxide layer, while the interior and lower sections showed minimal presence of oxide layer. This phenomenon could potentially be attributed to the varying surface areas of the specimens that came into contact with the air, consequently influencing the extent of oxidation. However, during the subsequent experimental process, it was discovered that after 7 days of specimen placement, despite the change in color, the uniaxial compressive strength and Young's modulus remained essentially unchanged.

Table 2 presents the dimensional and mass alterations of the sand 3D printed rock-like specimens across varying placement durations. Initially, the specimens exhibited mass values within the range of 279–284 g, while their density spanned from 1.417 to 1.442 g/cm³. Notably, after approximately 30 days of placement, the mass variation for the specimens was merely 1 g, underscoring their relative stability under room temperature conditions without necessitating any subsequent treatments. Moreover, the mass and density of the printed specimens in this study closely approximated the outcomes documented by Hodder et al. (2022).
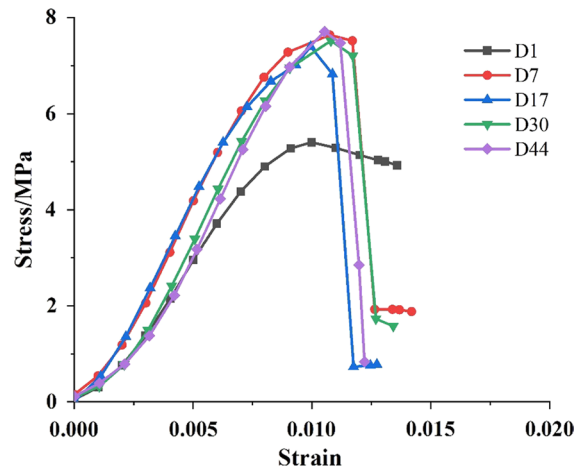

Fig. 6 Stress–strain curves of sand powder3D printed rock-like specimen with different placement times

Table 2 Weight and density of specimen with different placement time

Time	Number	Weight at the beginning (g)	Weight at the testing (g)	Change (g)	Density (g/cm³)
Day1	D1-1	279	279	0	1.422
	D1-2	283	283	0	1.427
	D1-3	280	280	0	1.422
Day7	D7-1	281	281	0	1.432
	D7-2	282	282	0	1.437
	D7-3	280	280	0	1.427
Day17	D17-1	280	280	0	1.427
	D17-2	283	283	0	1.422
	D17-3	278	278	0	1.417
Day30	D30-1	280	279	1	1.422
	D30-2	282	281	1	1.432
	D30-3	282	281	1	1.432
Day44	D44-1	280	279	1	1.437
	D44-2	282	281	1	1.442
	D44-3	284	283	1	1.442

3.2 Influence of placement time on mechanical properties of specimens

### 3.2.1 Analysis of stress–strain curves

Figure 6 illustrates the stress–strain curves of specimens with varying placement times. The graph indicates that each specimen undergoes distinct stages, including compaction, elastic deformation, unstable fracture progression, and post-peak behavior. With the exception of the specimen with a 1 day placement period, the mechanical property curves for the remaining specimen groups exhibit remarkable similarity.

(1) *Initial Loading Stage (Compaction Stage)* In this stage, all curves demonstrate a concave compaction phase. This phenomenon arises as the original microcracks and voids formed during the 3D printing process of sand-based rock-like specimens gradually close, leading to early non-linear deformation and compaction of the rock material.

(2) *Elastic Deformation and Stable Micro-Elastic Crack Development Stage* Following the compaction stage, stress–strain curves for all specimens enter an elastic deformation phase characterized by stable micro-elastic crack development. In this stage, the curves exhibit approximately linear behavior. Nonetheless, the stress increment for the specimen with a 1 day placement period is notably smaller compared to the other groups. This divergence is attributed to the abbreviated placement time for the 1 day placement specimen, causing the curing agent attached to the sand particles' surface within the specimen to remain incompletely reacted with the furan resin. This results in incomplete curing of the specimen, rendering its interior comparatively softer.

(3) *Unstable Fracture Development Stage* Subsequent to the elastic deformation stage, all curves enter an unstable fracture development phase. Here, internal cracks within the specimens continue to propagate until complete specimen failure occurs.

(4) *Post peak stage* Following the attainment of peak strength, the specimen's internal structure experiences damage, yet the specimen remains intact. As pressure continues to escalate, the 1 day placement specimen does not immediately fracture but undergoes plastic deformation. Notably, the post-peak load-bearing capacity of the 1 day placement specimen surpasses that of the other groups, indicative of greater resilience and reduced brittleness. This behavior could be attributed to the specimen's incomplete interior curing within the short time frame, resulting in a certain degree of viscosity and tension in the binder between the particles within the specimen.

Fig. 7 The UCS, peak strain, and Young's modulus changes of sand powder 3D printed rock-like specimens with different placement times
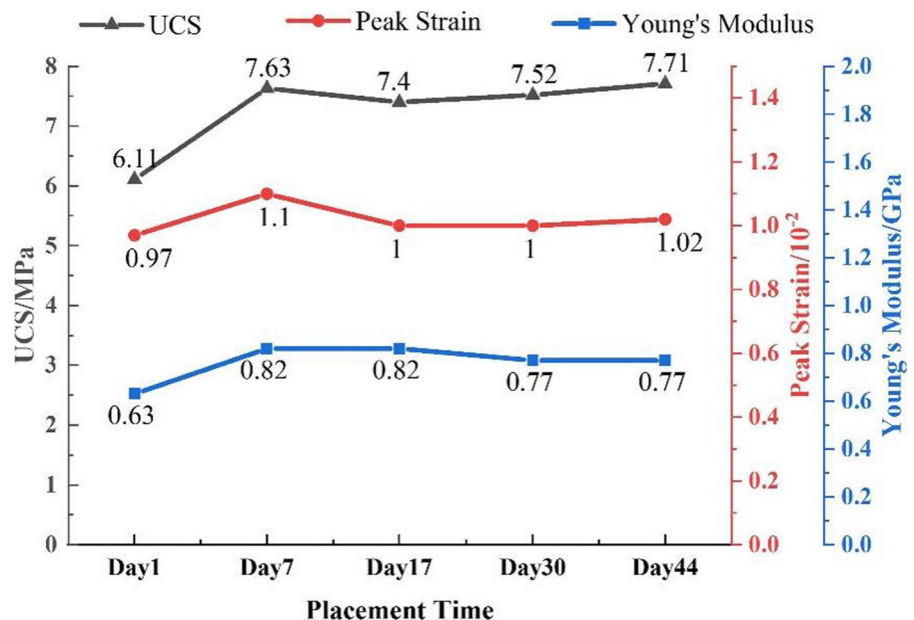
3.2.2 Influence of placement time on the mechanical properties of specimens

As shown in Fig. 7, the figure illustrates a comparison of the Uniaxial Compressive Strength (UCS), peak strain, and Young's modulus of sand powder 3D printed rock-like specimens with varying placement times. The graph reveals that alterations occur in UCS and Young's modulus with changing placement times, while the peak strain remains relatively consistent. In the initial stages of placement, there is a gradual increment in both UCS and Young's modulus as placement time lengthens. The average UCS rises from 6.11 to 7.38 MPa, and the average Young's modulus elevates from 0.63 to 0.84 GPa. This constitutes an average increase of 20.79% in UCS and 33.33% in Young's modulus. After approximately 7 days of placement, UCS and Young's modulus stabilize. This phenomenon is predominantly due to the strengthening of the bonding agent amidst the particles within the specimens over time. Within 1 day of placement, the intergranular bonding material attains a certain strength despite not being fully reacted. Following 7 days of placement, the bonding neck's strength between sand particles progressively heightens, eventually reaching a plateau. However, as placement time extends, the UCS of sand powder 3D printed rock-like specimen experiences minimal fluctuations. This outcome arises from the consistent printing substrate and parameters employed across each specimen group. Consequently, the binder quantity for each sand layer during printing remains comparable, yielding similar numbers of bonding necks and roughly equivalent porosity within the specimens. Variability primarily lies in the bonding strength between particles. Therefore, under the same loading rate, the time required for specimen failure remains roughly consistent.

3.2.3 Failure mode

The mechanical behavior and failure patterns of sand powder 3D printed rock-like specimens bear a striking resemblance to the mechanical attributes and failure modes observed in natural rocks (Kong et al. et al. 2019; Hodder et al. 2022). Thus, this section primarily delves into the distinctions in failure modes across specimens with varying placement durations. As shown in Fig. 8, upon scrutinizing the

Fig. 8 The uniaxial compression failure morphology of sand powder 3D printed rock-like specimens with different placement times
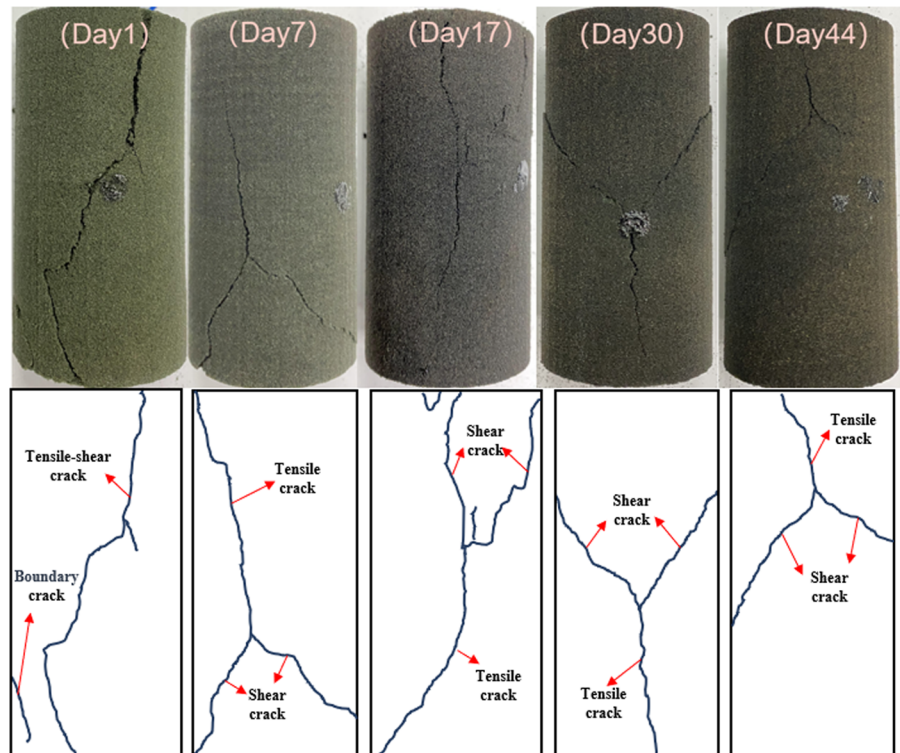
failure morphology of specimens exposed to different placement times, some distinct patterns emerge. Specimens subjected to 1 day of placement predominantly exhibit tensile failure, whereas the remaining groups showcase tensile-shear failure. Notably, a characteristic Y-shaped fracture pattern, referred to as the "end cap cone," manifests at the center. This phenomenon involves the development of a conical failure zone at the specimen's end (Kong et al. 2018a, b). The compression process gives rise to multiple crack surfaces, accompanied by the continuous detachment of sand particles from the specimen's surface. The fracture process witnesses a substantial shedding of sand particles from the crack surface. This phenomenon results from the continuous fracturing of bonding necks between sand particles within the specimen during compression, culminating in the detachment of these particles. The diversity in failure modes observed in sand powder 3D printed rock-like specimens with different placement times strikingly mirrors the failure modes found in certain weakly cemented sandstones under natural conditions, thereby substantiating the aptitude of sand powder 3D printed rock-like specimens in emulating various types of natural rock behaviors.

3.2.4 Acoustic emission characteristics

Within this investigation, acoustic emission monitoring was applied to specimens subjected to varying placement times, complemented by stress-time curves, facilitating an examination of internal transformations throughout deformation and failure. This analysis hinged on two distinct parameters: cumulative ring count and acoustic emission energy. Due to the consistent acoustic emission traits displayed by specimens within the same group, this study opted to analyze representative data from each specimen group. As shown in Fig. 9, the stress-time curves are juxtaposed with corresponding plots of cumulative ring count and acoustic emission energy for these illustrative specimens with differing placement times.

As shown in Fig. 9a, it is evident that the acoustic emission energy of the 1-day placement specimen experiences a mild rise during the compaction stage, although it maintains a relatively low level of magnitude. This phenomenon arises from the incompleteness of internal curing within the 1 day placement specimen, resulting in comparatively feeble bonding

among the powdered sand particles within the specimen. As stress is applied, primary cracks and voids within the specimen slowly seal, engendering slight friction amid the powdered sand particles. Throughout the elastic deformation phase and the ensuing unstable fracture development stage, the acoustic emission energy of the specimen undergoes gradual diminishment, while the cumulative ringing count progressively increases. This trend emerges as the newly formed cracks, post-compaction, are not yet fully developed, yielding a decreased incidence of acoustic emission events. This phenomenon precipitates a "quiet period" prior to the peak. Following the peak stress point, the 1 day placement specimen's compressive strength gradually wanes due to the partial curing of the bonding neck connecting the powdered sand particles within the specimen. Consequently, the gradual initiation and expansion of internal cracks ensue, gradually elevating the acoustic emission energy and amplifying the growth rate of the cumulative ringing count. As microcracks accumulate internally, the specimen eventually gives rise to macroscopic cracks. In a critical juncture, the 1 day placement specimen abruptly collapses under the applied stress, prompting a sharp surge in acoustic emission energy and a swift escalation in the cumulative ringing count.

During the compaction stage, the acoustic emission events within the specimen gain prominence as primary cracks and voids internally converge and adjust under the influence of stress, thereby generating elastic waves. During the compaction stage, the acoustic emission events within the specimen gain prominence as primary cracks and voids internally converge and adjust under the influence of stress, thereby generating elastic waves. Progressing from the elastic deformation phase through to the non-elastic stable fracture development stage and the subsequent unstable fracture development stage, the acoustic emission energy consistently diminishes, while the cumulative ringing count exhibits a gradual augmentation. This phenomenon arises as the primary cracks and voids within the specimen continue to compact. Upon reaching the peak stress, the specimen doesn't immediately rupture; instead, it endures an additional loading period before eventual fracture. Upon fracture, there is a rapid surge in acoustic emission energy. Post-fracture, while the acoustic emission energy swiftly diminishes, it doesn't descend to zero. Meanwhile, the cumulative ringing count undergoes

Fig. 9 Stress-time and corresponding acoustic emission energy, cumulative ringing count curves
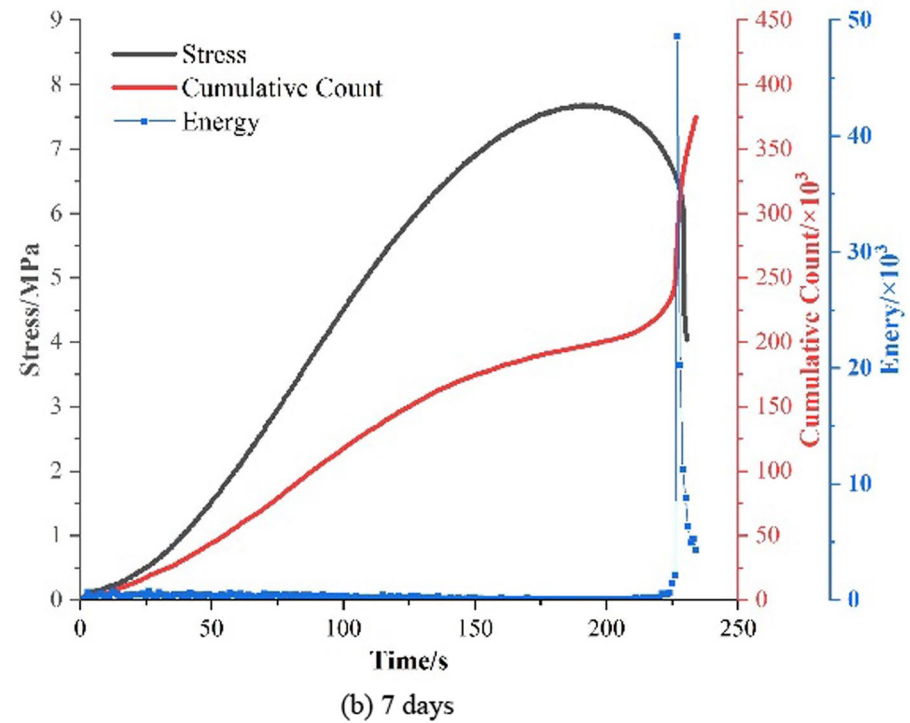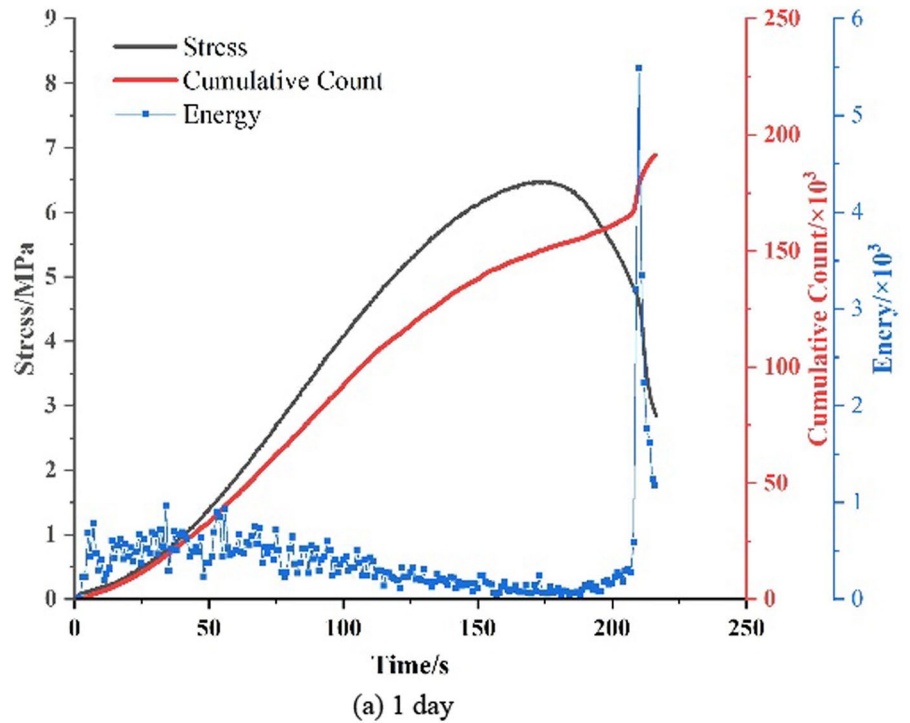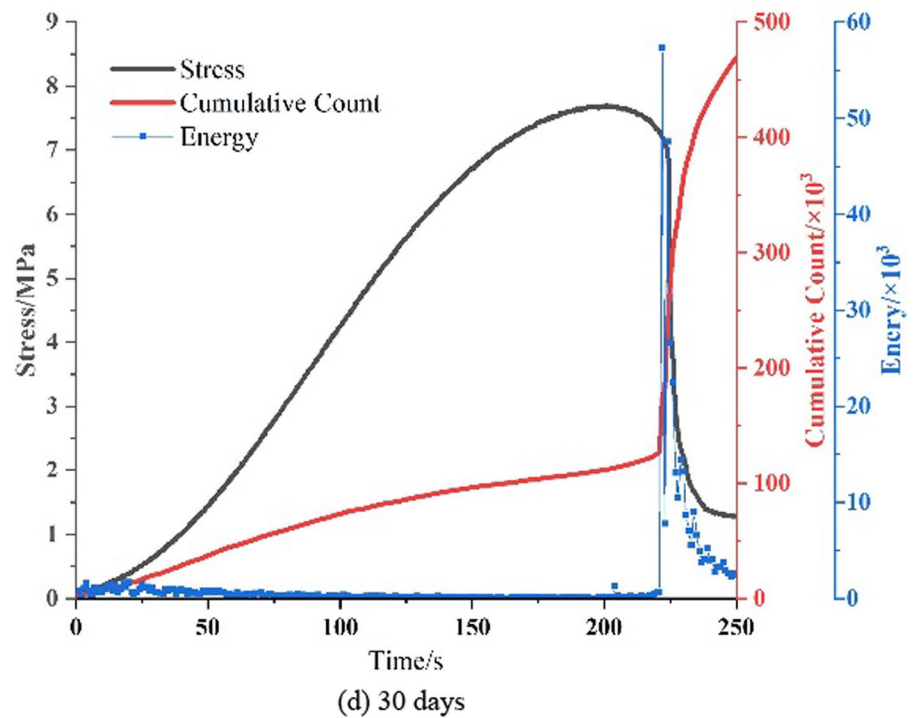

(a) 1 day

(b) 7 days

Fig. 9 (continued)

(c) 17 days

(d) 30 days

Fig. 9 (continued)

(e) 44 days
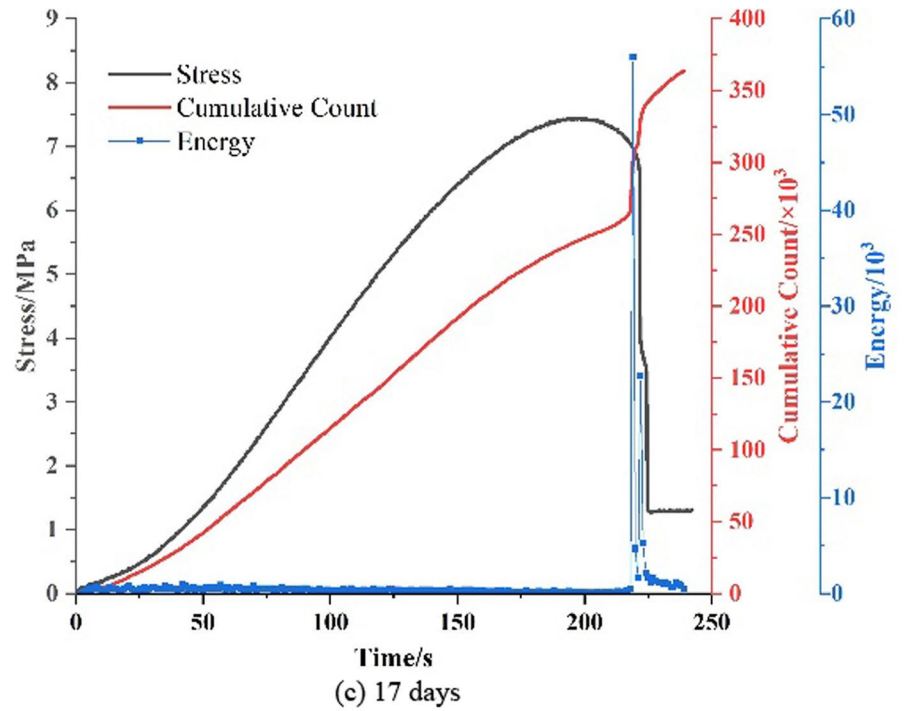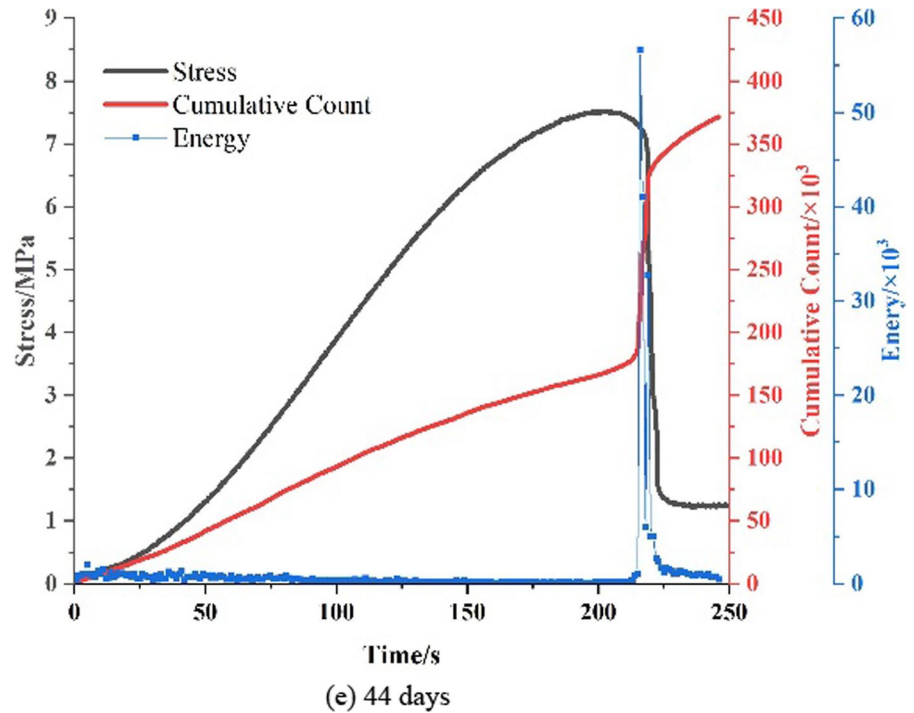
a rapid escalation, followed by a sustained incremental growth. This behavior arises due to the persistent friction and particle detachment within the specimen, particularly after the formation of the macroscopic fracture surface.

With the exception of the specimen placement for 1 day, the acoustic emission traits of the remaining specimen groups exhibit considerable similarities. It's important to note that the cumulative ringing count remains consistent at the failure point for specimens placed for 7 days. This observation suggests that the internal configuration of the sand powder 3D printed rock-like specimens retains its constancy following a placement duration of around 7 days or beyond. This, in turn, indicates that the fundamental internal structure of the sand powder 3D printed rock-like specimens undergoes minimal change after undergoing placement for roughly 7 days or longer.

Fig. 10 Rock slices and SEM

(a) Rock slices

(b) Apreo S HIVac
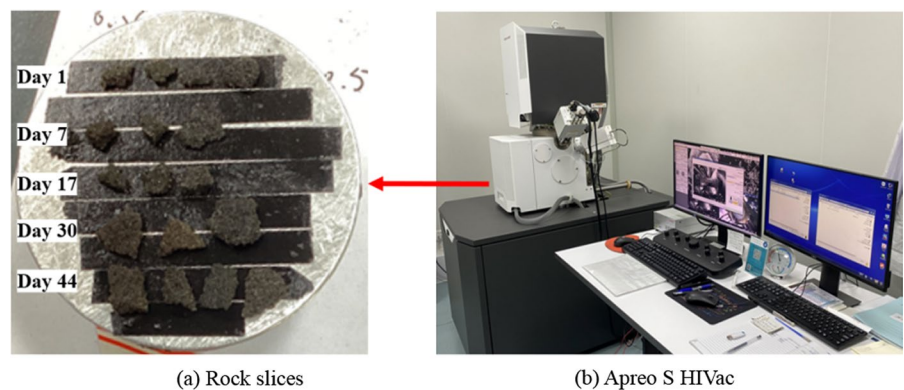
3.3 Microscopic fracture mechanism

Following test completion, rock slices are extracted from the fractured surfaces of the specimens within each group and subjected to scanning using a Scanning Electron Microscope (SEM) at magnifications ranging from 200 to 1000 times. The scanning electron microscope used was the Apreo S HIVac with high-resolution scanning and compound lenses, as shown in Fig. 10. Through an analysis encompassing the foundation principles of sand powder 3D printing technology and the outcomes gleaned from microscopic scanning, the impact of varying placement times on the microscopic fracture mechanism of the specimens is meticulously investigated.

The curing mechanism of furan resin involves various processes, including electrophilic substitution, D-A ring addition curing mechanism, as well as oxidative and non-oxidative cracking addition curing mechanisms (Xia et al. 2014). Among these, electrophilic substitution and D-A ring addition are the primary mechanisms. The core of the curing mechanism revolves around the acid-catalyzed polymerization reaction of furan resin. This reaction involves two dehydration condensation reactions that lead to the extension of linear molecular chains. The outcome is the formation of an acid and alkali-resistant, insoluble, and non-melting black solid, as shown in Fig. 11. This solid constitutes the primary bonding structure between sand particles (Primkulov et al. 2017). This material plays a pivotal role in the curing process. The bonding configuration of these necks holds substantial sway over both the mechanical attributes of the sand powder 3D printed rock-like specimens and the intricate structure of the specimens' voids (Wang et al. 2022a; b).

SEM images were captured at a magnification of 500 times and were carefully selected to analyze void spaces at the fracture sites of specimens with different placement durations. EM images captured at an appropriate magnification of 500 times were meticulously chosen to extract the void spaces at the fracture sites of specimens subjected to varying placement durations. The entirety of fracture surface slices for specimens with different placement times were systematically scanned at 200 times magnification, as well as locally examined at 1000 times magnification (indicated by the blue circle, signifying sand particles), offering a comprehensive view (as shown in Fig. 12). Predominantly, the primary void type in the sand powder 3D printed rock-like specimens is intergranular voids, and there is no observable instance of binder infiltrating these voids. Across the overall morphology of the fracture surfaces for each group of specimens, particles are distinctly discernible, accompanied by prominent intergranular voids. The macroscopic structure and microscopic composition of the fracture surface for specimen placement over different durations remain strikingly uniform. This observation reinforces that placement time does not significantly alter the inner framework of the specimens. The internal fracture surface of specimen placement for only 1 day is notably soft and pliable, with a perceivable dampness. This phenomenon arises from the furan resin and curing agent between the sand particles existing in an incomplete "gel state" due to inadequate reaction time. The reaction remains ongoing and the generated moisture has yet to dissipate. Consequently, the compressive strength of the 1 day placement specimen is substantially lower than that of the other groups. Over time, as the furan resin
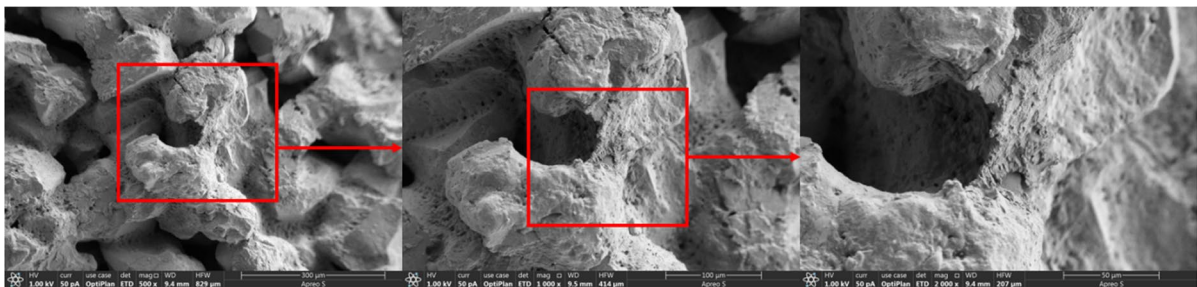

Fig. 11 Black insoluble and non-melting substance (binding neck)

and curing agent within the specimen achieve full reaction, interparticle bonding necks solidify and internal moisture evaporates. This progression results in the specimen's strength increment and subsequent stabilization.

SEM images were captured at a magnification of 500 times and were carefully selected to analyze void spaces at the fracture sites of specimens with different placement durations. Fracture surface slices from specimens with different placement times were systematically scanned at 200 times magnification. Additionally, local examinations were conducted at 1000 times magnification, as indicated by the blue circles highlighting sand particles, providing a comprehensive view (see Fig. 12).

4 Discussion

Through a thorough and comprehensive comparative analysis encompassing molding traits and mechanical attributes of sand powder 3D printed rock-like specimens alongside various conventional rock specimens, a range of significant advantages become evident. Notably, sand powder 3D printed rock-like specimens exhibit rapid molding speed. They also demonstrate elasto-plastic mechanical attributes comparable to authentic coal-rock specimens. The capability to simulate intricate internal fractures, unwavering stability, obviating the necessity for prolonged maintenance, and notable cost-effectiveness in contrast to their conventional counterparts. Figure 13 shows the comparison between different printing techniques' specimens and real coal-rocks.

In contrast to sand powder 3D printed rock-like specimens, traditional casting molded specimens and cement-based printed specimens have mechanical attributes similar to authentic rocks and can simulate a broader spectrum of rock types. However, they are encumbered by certain limitations. Traditional casting necessitates a minimum of 28 days for curing, and both casting molding and cement-based specimens fall short in effectively replicating intricate internal fractures, thereby compromising their accuracy. Conversely, when juxtaposed with SLS rock specimens and gypsum counterparts, sand powder 3D printed rock-like specimens emerge as possessing mechanical characteristics more closely aligned with genuine coal-rock specimens.

Through an investigation into the impact of various placement time on the mechanical characteristics of sand powder 3D printed rock-like specimens, a suitable placement time has been established. The study reveals that the mechanical attributes of the specimens stabilize after around 7 days of placement, presenting a favorable scenario for the utilization of sand powder 3D printing technology in laboratory testing. Nonetheless, it is important to acknowledge that the present research carries certain limitations, encompassing the following aspects:

(1) Similarity in physical properties comparing to real rocks

As a category of rock-like material, it is imperative to ascertain whether the fundamental elasto-plastic mechanical properties of 3D printed rock-like specimens closely correspond to those of the targeted simulated rock types. This alignment serves as a crucial prerequisite and foundation for conducting rock mechanics research utilizing this approach. The assessment criteria extend beyond mere strength and encompass parameters such as deformation modulus and post-peak characteristics.

(2) Generation and accuracy of fractures.

The primary objective of employing 3D printing technology revolves around crafting rock-like specimens that faithfully replicate the intrinsic flaws, including fractures and voids, present within the authentic rock formations. Hence, subsequent to verifying the mechanical attributes akin to coal rock-like materials, a pivotal concern arises—namely, devising methodologies to fabricate fractured coal-rock specimens in accordance with the spatial attributes of real fractures encountered in the field. This pursuit is instrumental in facilitating pertinent investigations into the mechanics of fractured rock masses.

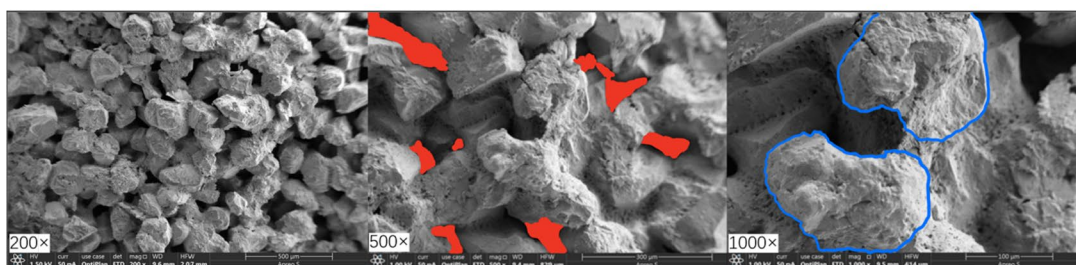(3) Uncontrolled properties through printing materials and parameters

The field of mining engineering encounters a diverse range of rock types and strengths within the rock mass. As a nascent category of rock material, it is imperative to elucidate the influence of materials, parameters, and processes on the mechanical traits of
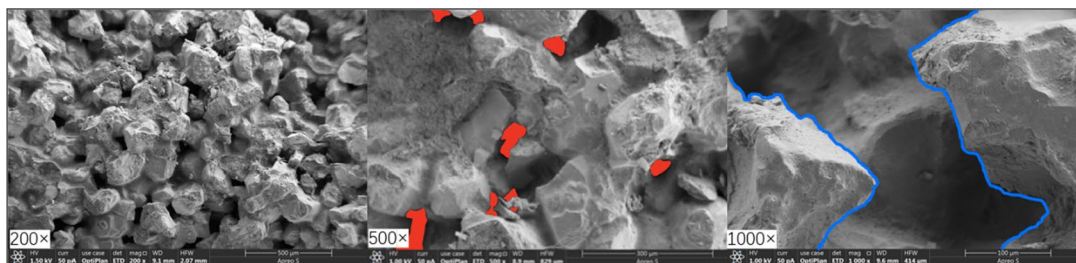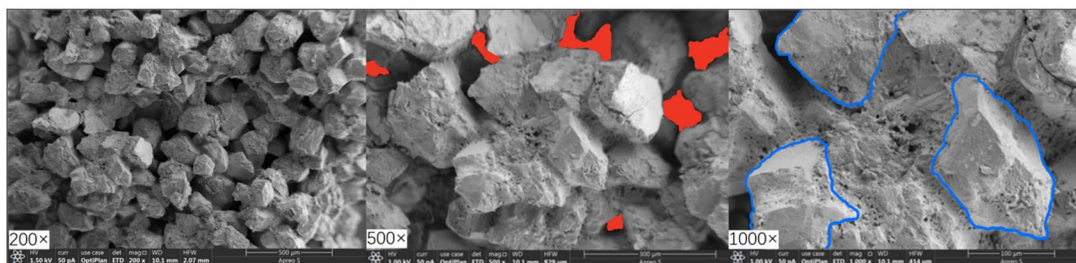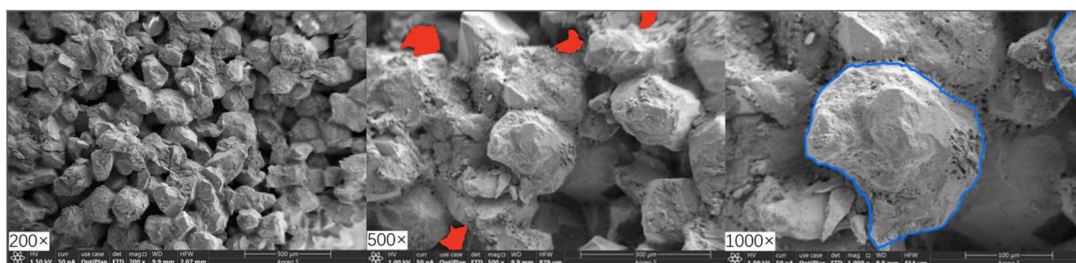
(a) 1 day
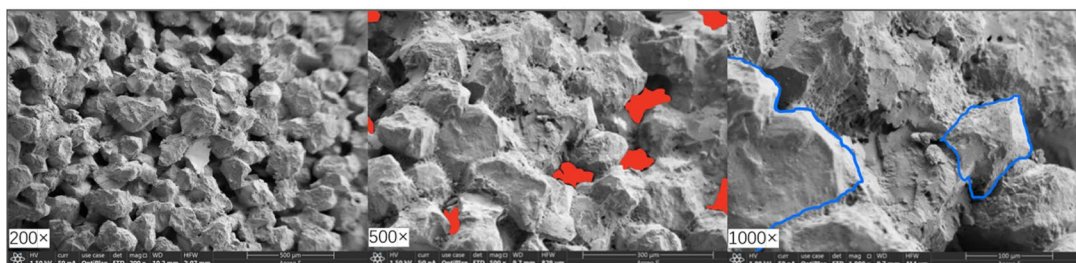
(b) 7 days

(c) 17 days

(d) 30 days

(e) 44 days

fabricated specimens. Achieving regulated mechanical properties for these specimens is pivotal, enabling the creation of rock-like samples that align with the mechanical attributes of distinct target coal-rock formations. Presently, the strength of sand powder 3D printed rock-like specimens exhibits limitations, allowing simulation primarily of specific natural soft rock compositions.

5 Conclusion

This study explores the influence of different placement times on the mechanical properties of sand powder 3D printed rock-like specimens. By combining uniaxial compression tests with acoustic emission (AE) technology, we investigate how varying placement times impact both the mechanical characteristics and acoustic emission patterns of the specimens. Additionally, through the utilization of scanning electron microscopy, we delve into changes within the internal microstructure of these specimens, shedding light on the intricate relationship between placement time and the inherent mechanical properties of sand powder 3D printed rock-like specimens. The main research findings of this study are as follows:

(1) After placement, sand powder 3D printed rock-like specimens exhibit consistent macroscopic physical attributes and a homogenous internal structure. The mass of the specimens remains relatively constant over time, with a mere 1 g reduction in mass observed after 30 days of placement. While the surface color of the specimen undergoes changes over time, the alterations in color and the degree of oxidation on the surface insignificantly impact the mechanical characteristics of the specimens.

(2) Sand powder 3D printed rock-like specimens demonstrate a degree of strength following 1 day of placement, albeit retaining some plasticity post-peak. Subsequent to approximately 7 days of placement, the uniaxial compressive strength (UCS) and Young's modulus exhibit stability, characterized by an average UCS increase of 20.79% and an average Young's modulus increase of 33.33%. Consequently, the mechanical attributes of the specimens remain essentially consistent after being subjected to around 7 days of room temperature placement.

(3) The integration of acoustic emission monitoring and scanning electron microscopy of fracture surfaces has unveiled a significant observation: specimens placement for more than 7 days exhibit uniform internal structures and consistent attributes. This discovery underscores the stability inherent in sand powder 3D
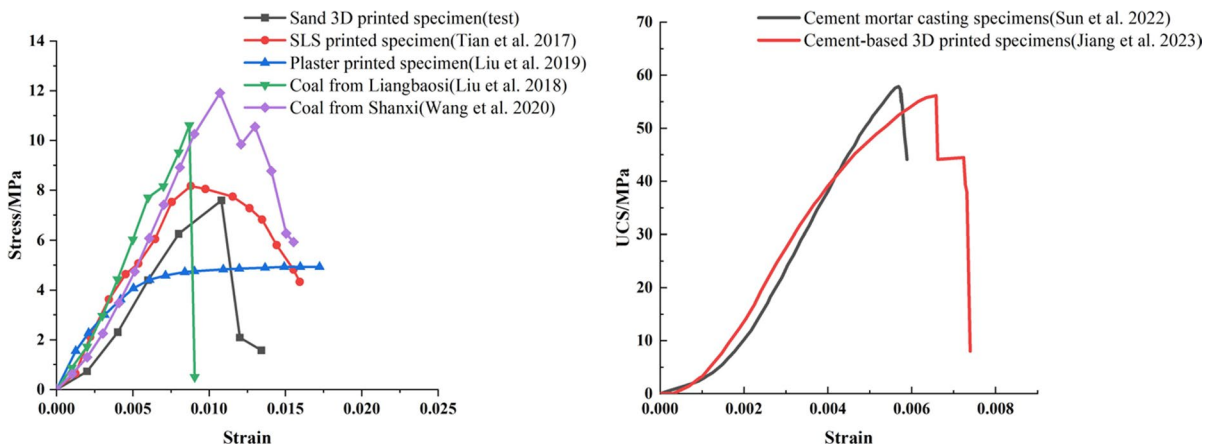

Fig. 13 Comparison between different printing techniques' specimens and real coal-rocks

printing technology throughout the entirety of the printing process.

(4) Upon comparing with authentic rock specimens and alternative rock-like materials, sand powder 3D printed rock-like specimens provide several notable advantages. These encompass swift molding, mechanical properties closely resembling those of genuine coal-rock specimens, the capability to craft intricate internal fractures, freedom from extensive maintenance requirements, and cost-effective production.

Availability of data and materials All of the material is owned by the authors and/or no permissions are required.

Declarations

Ethics approval and consent to participate This research did not involve human subjects or animal experimentation. As a result, no ethics approval was required for this study. Any potential conflicts of interest were disclosed and managed in accordance with the ethical standards of our institution.

Consent for publication I confirm the corresponding author has read the journal policies and submit this manuscript in accordance with those policies.

Competing interests The authors declare no competing interests.

References

Almetwally AG, Jabbari H (2020) Experimental investigation of 3D printed rock samples replicas. J Nat Gas Sci Eng 76:103192. https://doi.org/10.1016/j.jngse.2020.103192

Barbosa K, Hodder K, Yahyaei M (2022) Experimental study on mechanical properties of 3D-printed specimens of iron oxide, quartz, and bedded composites under uniaxial compression and indirect tensile strength. 3D Print Addit Manuf

Barton N (1972) A model study of rock-joint deformation. Int J Rock Mech Min Sci Geomech Abstr 9(5):579–582. https://doi.org/10.1016/0148-9062(72)90010-1

Barton N, Bandis S, Bakhtar K (1985) Strength, deformation and conductivity coupling of rock joints. Int J Rock Mech Min Sci Geomech Abstr 22(3):121–140. https://doi.org/10.1016/0148-9062(85)93227-9

Bertuzzi R, Pells P (2002) Geotechnical parameters of Sydney sandstone and shale. Aust Geomech News J Aust Geomech Soc 37(5):41–54. https://doi.org/10.3316/informit.812689394955021

Cacciari P, Futai M (2022) A practical method for estimating the volumetric intensity of non-persistent discontinuities on rock exposures. Rock Mech Rock Eng 55:6063–6078. https://doi.org/10.1007/s00603-022-02966-w

Cao P, Liu T, Pu C, Lin H (2015) Crack propagation and coalescence of brittle rock-like specimens with pre-existing cracks in compression. Eng Geol 187:113–121. https://doi.org/10.1016/j.enggeo.2014.12.010

Cao Rh, Cao P, Lin H et al (2016) Mechanical behavior of brittle rock-like specimens with pre-existing fissures under uniaxial loading: experimental studies and particle mechanics approach. Rock Mech Rock Eng 49:763–783. https://doi.org/10.1007/s00603-015-0779-x

Cao R, Cao P, Lin H et al (2019) Crack initiation, propagation, and failure characteristics of jointed rock or rock-like specimens: a review. Adv Civ Engz. https://doi.org/10.1155/2019/6975751

Dyskin A, Sahouryeh E et al (2003) Influence of shape and locations of initial 3-D cracks on their growth in uniaxial compression. Eng Fract Mech 70(15):2115–2136. https://doi.org/10.1016/S0013-7944(02)00240-0

Fedrizzi R, de Ceia M et al (2018) Artificial carbonate rocks: synthesis and petrophysical characterization. J Pet Sci Eng 163:303–310. https://doi.org/10.1016/j.petrol.2017.12.089

Feng X, Haimson B, Li X et al (2019) ISRM suggested method: determining deformation and failure characteristics of rocks subjected to true triaxial compression. Rock Mech Rock Eng 52:2011–2020. https://doi.org/10.1007/s00603-019-01782-z

Gao Y, Wu T, Zhou Y (2021) Application and prospective of 3D printing in rock mechanics: a review. Int J

Miner Metall Mater 28:1–17. https://doi.org/10.1007/s12613-020-2119-8

Gehlin S (1998) Thermal response test: in situ measurements of thermal properties in hard rock. Luleå tekniska universitet

Gomez J, Chalaturnyk R, Zambrano-Narvaez G (2019) Experimental investigation of the mechanical behavior and permeability of 3D printed sandstone analogues under triaxial conditions. Transp Porous Media 129(2):541–557. https://doi.org/10.1007/s11242-018-1177-0

Goodman RE, Taylor RL, Brekke TL (1968) A model for the mechanics of jointed rock. J Soil Mech Found Div 94(3):637–659. https://doi.org/10.1061/JSFEAQ.0001133

Haeri H, Khaloo A, Marji M (2015) Experimental and numerical analysis of Brazilian discs with multiple parallel cracks. Arab J Geosci 8:5897–5908. https://doi.org/10.1007/s12517-014-1598-1

Hart R (2003) Enhancing rock stress understanding through numerical analysis. Int J Rock Mech Min Sci 40(7–8):1089–1097. https://doi.org/10.1016/S1365-1609(03)00116-3

Herget G, Unrug K (1976) In situ rock strength from triaxial testing. Int J Rock Mech Min Sci Geomech Abstr 13(11):299–302. https://doi.org/10.1016/0148-9062(76)91828-3

Hodder K, Sanchez-Barra A, Ishutov S (2022) Increasing density of 3D-printed sandstone through compaction. Energies 15:1813. https://doi.org/10.3390/en15051813

Jiang C, Zhao GF (2015) A preliminary study of 3D printing on rock mechanics. Rock Mech Rock Eng 48:1041–1050. https://doi.org/10.1007/s00603-014-0612-y

Jiang C, Zhao GF, Zhu J et al (2016a) Investigation of dynamic crack coalescence using a gypsum-like 3D printing material. Rock Mech Rock Eng 49:3983–3998. https://doi.org/10.1007/s00603-016-0967-3

Jiang Q, Feng X, Song L et al (2016b) Modeling rock specimens through 3D printing: tentative experiments and prospects. Acta Mech Sin 32:101–111. https://doi.org/10.1007/s10409-015-0524-4

Jiang L, Wu X, Wang Q, Feng H, Wu Q (2022) Mechanical characteristics of dynamic and static combined loading of sand powder 3D printed coal-like specimens. J China Coal Soc 47(03):1196–1207

Ju Y, Xie H, Zheng Z et al (2014) Visualization of the complex structure and stress field inside rock by means of 3D printing technology. Chin Sci Bull 59:5354–5365. https://doi.org/10.1007/s11434-014-0579-9

Ju Y, Wang L, Xie H et al (2017a) Visualization and transparentization of the structure and stress field of aggregated geomaterials through 3D printing and photoelastic techniques. Rock Mech Rock Eng 50:1383–1407. https://doi.org/10.1007/s00603-017-1171-9

Ju Y, Wang L, Xie H et al (2017b) Visualization of the three-dimensional structure and stress field of aggregated concrete materials through 3D printing and frozen-stress techniques. Constr Build Mater 143:121–137. https://doi.org/10.1016/j.conbuildmat.2017.03.102

Kim H, Lee J, Yazdani M et al (2018) Coupled viscous fluid flow and joint deformation analysis for grout injection in a rock joint. Rock Mech Rock Eng 51:627–638. https://doi.org/10.1007/s00603-017-1339-3

Kong L, Ostadhassan M, Li C et al (2018a) Can 3-D printed gypsum samples replicate natural rocks? An experimental study. Rock Mech Rock Eng 51:3061–3074. https://doi.org/10.1007/s00603-018-1520-3

Kong L, Ostadhassan M, Li C et al (2018b) Pore characterization of 3D-printed gypsum rocks: a comprehensive approach. J Mater Sci 53:5063–5078. https://doi.org/10.1007/s10853-017-1953-1

Kong L, Ostadhassan M, Hou X et al (2019) Microstructure characteristics and fractal analysis of 3D-printed sandstone using micro-CT and SEM-EDS. J Pet Sci Eng 175:1039–1048. https://doi.org/10.1016/j.petrol.2019.01.050

Kovari K, Tisa A, Einstein HH et al (1983) Suggested methods for determining the strength of rock materials in triaxial compression: revised version. Int J Rock Mech Min Sci Geomech Abstr. https://doi.org/10.1016/0148-9062(83)90598-3

Li D, Han Z, Sun X et al (2019) Dynamic mechanical properties and fracturing behavior of marble specimens containing single and double flaws in SHPB tests. Rock Mech Rock Eng 52:1623–1643. https://doi.org/10.1007/s00603-018-1652-5

Liu L, Deisman N, Chalaturnyk R (2022) Elastic stiffness modelling of opalinus clay based on laboratory measurements with implications for in-situ testing. Rock Mech Rock Eng 55(4):1823–1842. https://doi.org/10.1007/s00603-021-02768-6

Ma Q, Liu XL, Tan YL et al (2023) Numerical study of mechanical properties and microcrack evolution of double-layer composite rock specimens with fissures under uniaxial compression. Eng Fract Mech 289(2):109403. https://doi.org/10.1016/j.engfracmech.2023.109403

Mangs AD, Wagner NJ, Moroeng OM, Lar UA (2022) Petrographic composition of coal within the Benue Trough, Nigeria and a consideration of the paleodepositional setting. Int J Coal Sci Technol 9(1):35. https://doi.org/10.1007/s40789-022-00500-5

Nicksiar M, Martin CD (2012) Evaluation of methods for determining crack initiation in compression tests on low-porosity rocks. Rock Mech Rock Eng 45:607–617. https://doi.org/10.1007/s00603-012-0221-6

Niu Q, Jiang L, Li C et al (2023) Application and prospects of 3D printing in physical experiments of rock mass mechanics and engineering: materials, methodologies and models. Int J Coal Sci Technol 10:5. https://doi.org/10.1007/s40789-023-00567-8

Nizametdinov F, Nagibin A, Levashov V et al (2016) Methods of in situ strength testing of rocks and joints. J Min Sci 52:226–232. https://doi.org/10.1134/S1062739116020357

Perras M, Vogler D (2019) Compressive and tensile behavior of 3D-printed and natural sandstones. Transp Porous Med 129:559–581. https://doi.org/10.1007/s11242-018-1153-8

Primkulov B, Chalaturnyk J, Chalaturnyk R, Zambrano Narvaez G (2017) 3D printed sandstone strength: curing of furfuryl alcohol resin-based sandstones. 3D Print Addit Manuf. https://doi.org/10.1089/3dp.2017.0032

Song R, Wang Y, Ishutov S et al (2020) A comprehensive experimental study on mechanical behavior,

microstructure and transport properties of 3D-printed rock analogs. Rock Mech Rock Eng 53:5745–5765. https://doi.org/10.1007/s00603-020-02239-4

Sun W, Du H et al (2019) Experimental study of crack propagation of rock-like specimens containing conjugate fractures. Geomech Eng 17(4):323

Tang X, Zhang Y, Xu J et al (2022) Determining Young's modulus of granite using accurate grain-based modeling with microscale rock mechanical experiments. Int J Rock Mech Min Sci 157:105167. https://doi.org/10.1016/j.ijrmms.2022.105167

Tian W, Wang X, Yun W et al (2023) Study on mechanical properties of sand powder 3D printed rock-like specimens based on different post-processing methods. Rock Soil Mech 44(05):1330–1340+1352

Vălean C, Marşavina L, Mărghitaş M et al (2020) The effect of crack insertion for FDM printed PLA materials on Mode I and Mode II fracture toughness. Procedia Struct Integr 28:1134–1139. https://doi.org/10.1016/j.prostr.2020.11.128

Vogler D, Walsh SDC, Dombrovski E et al (2017) A comparison of tensile failure in 3D-printed and natural sandstone. Eng Geol 226:221–235. https://doi.org/10.1016/j.enggeo.2017.06.011

Wang Qi, Gao H, Jiang B et al (2021a) In-situ test and bolt-grouting design evaluation method of underground engineering based on digital drilling. Int J Rock Mech Min Sci 138:1365–1609. https://doi.org/10.1016/j.ijrmms.2020.104575

Wang B, Jin A, Sun H et al (2021b) Study on fracture mechanism of rough cross-jointed specimens with different angles based on 3D printing and DIC. Rock Soil Mech 42(02):439–450+461

Wang W, Zhao Y, Jiang L et al (2022a) Preliminary study on size effect of fractured rock mass with sand powder 3D printing. Processes 10(10):1974. https://doi.org/10.3390/pr10101974

Wang Y, Li S, Song R et al (2022b) Effects of grain size and layer thickness on the physical and mechanical properties of 3D-printed rock analogs. Energies 15:7641. https://doi.org/10.3390/en15207641

Xia Y, Lin X, Du Z et al (2014) Research progress on furan resin curing system and its curing mechanism. Mater Rep 28(19):79–83

Xu Q, Jiang L, Ma C, Niu Q, Wang X (2021) Effect of layer thickness on the physical and mechanical properties of sand powder 3D printing specimens. Front Earth Sci 9:763202. https://doi.org/10.3389/feart.2021.763202

Yan Z, Dai F, Zhu J et al (2021) Dynamic cracking behaviors and energy evolution of multi-flawed rocks under static pre-compression. Rock Mech Rock Eng 54:5117–5139. https://doi.org/10.1007/s00603-021-02564-2

Zhang K, Li N (2022) A new method to replicate high-porosity weak rocks subjected to cyclic freezing-thawing: sand 3D printing and digital image correlation explorations. Int J Rock Mech Min Sci 157:105174. https://doi.org/10.1016/j.ijrmms.2022.105174

Zhang K, Zhang K, Jin K et al (2023) Influence of intermittent opening density on mechanical behavior and fracture characteristics of 3D-printed rock. Theor Appl Fract Mech 124:103764. https://doi.org/10.1016/j.tafmec.2023.103764

Zhao Y, Jiang L, Li C et al (2023) Experimental investigation into the mechanical behavior of jointed soft rock using sand powder 3D printing. Rock Mech Rock Eng 56:5383–5404. https://doi.org/10.1007/s00603-023-03346-8

Zheng Y, Liu J, Zhang B (2019) An investigation into the effects of weak interfaces on fracture height containment in hydraulic fracturing. Energies 12:3245. https://doi.org/10.3390/en12173245

Zhou T, Zhu J, Xie H (2020) Mechanical and volumetric fracturing behaviour of three-dimensional printing rock-like samples under dynamic loading. Rock Mech Rock Eng 53:2855–2864. https://doi.org/10.1007/s00603-020-02084-5

Zhu JB, Zhou T, Liao ZY et al (2018) Replication of internal defects and investigation of mechanical and fracture behaviour of rock using 3D printing and 3D numerical methods in combination with X-ray computerized tomography. Int J Rock Mech Min Sci 106:198–212. https://doi.org/10.1016/j.ijrmms.2018.04.022